CREATED USING THE RSC LaTeX PCCP ARTICLE TEMPLATE – SEE www.rsc.org/electronicfiles FOR DETAILS

Evolution Study of Calcium Phosphate Precipitation in Hanging Drop Vapour Diffusion by In Situ Raman Microspectroscopy

Gloria Belén Ramírez-Rodríguez,[a] José Manuel Delgado-López*,[a] and Jaime Gómez-Morales[a]

Received Xth XXXXXXXXXX 20XX, Accepted Xth XXXXXXXXX 20XX
First published on the web Xth XXXXXXXXXX 200X
DOI: 10.1039/b000000x

The time-evolution of calcium phosphate precipitation by vapour diffusion has been studied by *in situ* Confocal Raman Microspectroscopy. A hanging drop configuration within a device known as "crystallisation mushroom" was employed in order to improve the Raman signal coming from growing crystals. This innovative methodology allowed to identify and follow the evolution of the precipitates formed at different areas of the drops containing mixed solutions of $Ca(CH_3COO)_2$ and $(NH_4)_2HPO_4$ due to the diffusion of CO_2 and NH_3 gases released from NH_4HCO_3 solutions at different concentrations (30 mM, 100 mM and 2 M). Time-dependent *in situ* Raman spectra indicated that amorphous calcium phosphate (ACP) was the first precipitate appearing just after mixing the Ca- and PO_4-containing solutions. Few minutes later, it transformed to dicalcium phosphate dihydrate (DCPD). The lifetime of DCPD strongly depends on the concentration of the NH_4HCO_3 solutions and thus on the pH increase rate. The pathway for the phase transformation from ACP to DCPD and then to octacalcium phosphate (OCP) followed a dissolution-reprecipitation mechanism. Additionally, OCP acted as temporal template for the heterogeneous nucleation and crystallization of biomimetic carbonate-apatite nanocrystals. The characterisation by TEM, XRPD and Raman spectroscopy of the freeze-dried powders obtained after seven days confirmed that OCP and carbonate-apatite nanocrystals (cAp) were the remaining phases when using 30 mM and 100 mM NH_4HCO_3 solutions. By contrast, working with the highest NH_4HCO_3 concentration the system evolved to the precipitation of elongated calcite crystals.

1 Introduction

Calcium orthophosphates have special relevance in biomineralization and biomedical fields because of their presence in mineralized tissues of mammals and their wide variety of applications[1] ranging from biomimetic bone graft and tissue regeneration to carriers matrices of drugs and proteins. In the last years a huge number of researches on the crystallisation process of these compounds have been carried out in order to analyse the mechanisms of precipitation and stability of each calcium phosphate phase (CaP).[2–13] Twelve biologically relevant CaP have been reported.[13] Among them, hydroxyapatite ($Ca_5(PO_4)_3(OH)$, HA), the thermodynamically most stable one under physiological conditions, represents the model compound of the inorganic constituent of bone, teeth and many pathological calcifications.[14,15] Bone apatites are non-stoichiometric calcium and OH deficient nanosized crystals doped with carbonate (4-6 w/w%) and different foreign ions such as Na (0.9%) and Mg (0.5%), among others.[16,17] Other phases such as dicalcium phosphate dihydrate ($CaHPO_4{\cdot}2H_2O$, brushite, DCPD) and octacalcium phosphate ($Ca_8H_2(PO_4)_6{\cdot}5H_2O$, OCP) are usually found in more acidic solutions.[18] Both DCPD and OCP have been suggested as possible metastable precursors in the formation of apatite. This may occur by the precipitation of DCDP and/or OCP followed by its transformation to a more apatitic phase.[13,18]

Several strategies to crystallise biomimetic nanosized apatite crystals have been reported including solid state reactions, co-precipitation, sol-gel synthesis, microemulsions, pyrolysis of aerosols, microwave precipitation and thermal decomplexing, among others.[19–30] Recently, we reported a novel methodology to precipitate biomimetic carbonate-apatite nanoparticles (cAp) and other CaP by sitting drop vapour diffusion (SDVD) micromethod both in the absence and in the presence of additives (aminoacids with different isoelectric points).[31–33] To do so, the "crystallisation mushroom" consisting in a specially designed environmental chamber was used. Additionally, SDVD micromethod was employed several times to carry out in vitro studies of $CaCO_3$ at different conditions.[34–36] Contemporaneously to our apatite crystallisation studies, vapour diffusion using millilitre scale vessels and 1 L desiccators was also tested by other authors to obtain carbonate-apatite nanoparticles.[19,20] The main features of the SDVD method are the following: i) the control of the rate of gas diffusion (NH_3 and CO_2) by changing the concentration of NH_4HCO_3 solution to make possible to regulate the pH increase until it reaches an asymptotic value, and as a con-

[a]*Laboratorio de Estudios Cristalográficos, IACT (CSIC-UGR), Avenida de las Palmeras, 4, 18100 Armilla, Granada, Spain. Fax: +34 958 55 26 20; Tel: +34 958 23 00 00 (*) E-mail: jmdl@lec.csic.es*

sequence, the rate of drops supersaturation, ii)the confinement of the nucleation in drops that closely resemble the in vivo microenvironments where biominerals are deposited, iii) the possibility to perform several experiments per run and iv) the doping of the apatite precipitate with CO_3^{2-} by means of the diffusion of CO_2 gas. The main drawback is the monitoring of the phase transformation either without stopping the precipitation process sequentially or performing different experiments as a function of time since valuable information of the early stages of CaP precipitation can be lost, as it occurred in previous works.[19,20,26,31–33] To solve this, we propose the use of vapour diffusion in a hanging drop configuration for the temporal monitoring of the process by means of a non-invasive spectroscopic technique, such as Confocal Raman Microspectroscopy.

Indeed, Raman Spectroscopy is a powerful tool for the chemical characterisation of different materials. Raman spectrometers, coupled to a confocal microscope, isolate the scattered light originated from the illuminated spot on the sample, and efficiently eliminate the contributions from out-of-focus zones improving the rejection of stray light and the z-spatial resolution. Such configuration can provide information about the process occurring at different areas of the solution. Moreover, due to the fact that water molecules are weak scatterers of visible light, it shows a low sensitivity to interference from water. These facts make this technique particularly suitable for *in situ* characterisation of solid samples growing in aqueous solutions without altering the sample.[37,38]

Therefore, the present work is focused on the study of the precipitation of CaP by hanging drop vapour diffusion (HDVD) micromethod by *in situ* Raman spectroscopy attached to confocal microscopy. The implementation of this configuration allows us to record the whole process of CaP transformation until attaining the apatite phase but without altering it or arresting the process, as occurred in previous works.[19,20,22–24,26–29] The aim is to prove the suitability of this technique to characterise the CaP precipitation at the earliest stages and its relation to the pH, the lifetime of metastable phases, and the role of the metastable precursor phase in the formation of apatites with nanosized dimensions.

2 Experimental

2.1 Materials

The solutions were prepared with ultrapure water (0.22 μS, 25 °C, MilliQ©, Millipore) and high purity chemical reagents, ammonium bicarbonate (NH_4HCO_3, 99% pure), ammonium phosphate dibasic ($(NH_4)_2HPO_4$, 99% pure) and calcium acetate ($Ca(CH_3COO)_2$, 99% pure) purchased from Sigma-Aldrich.

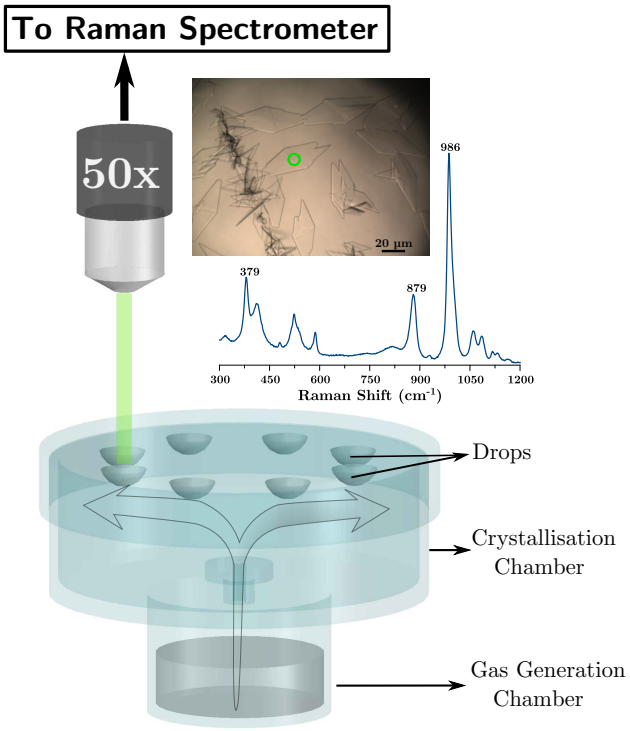

Fig. 1 Schematic view of the "crystallisation mushroom". The hanged drops can be analysed *in situ* by confocal Raman microspectroscopy. In fact, the image of the inset shows DCPD crystals and the corresponding Raman spectrum of the marked crystal with peaks appearing at ca: 379, 879 and 986 cm^{-1}.

2.2 Crystallisation method

HDVD experiments were performed in the "crystallisation mushroom" (Triana Science & Technology, S.L.), a device composed of two glass chambers connected each other through a hole of 6 mm diameter to allow the vapour diffusion (Figure 1). 1.5 mL of NH_4HCO_3 solution at different concentrations (30 mM, 100 mM and 2 M) was introduced in the gas generation chamber, while eight drops (1:1 v/v, 20 μL) containing 50mM $Ca(CH_3COO)_2$ + 30mM $(NH_4)_2HPO_4$ (Ca/P=5/3) were placed in the glass cover of the crystallisation chamber. The device was carefully sealed with silicon grease and paraffin to avoid the loss of gases (CO_2 and NH_3) released by the decomposition of the NH_4HCO_3 solution. The diffusion of NH_3 through the drops caused a gradual increase of their pH until it reached an asymptotic value. The experiments were performed at 20 °C and 1 atm.

The hanging drop compared to the sitting drop configuration does not only reduce the working distance but also allows to better focus on the crystals either at the drop/glass interface or in a focal plane inside the drop. Moreover, for the hanging drop configuration, Raman photons dispersed from crystals in-

This journal is © The Royal Society of Chemistry [year]

side the drop go back to the detector through a planar interface (drop/glass). Hence, the loss of Raman photons is considerably lower than in the sitting drop configuration where they pass through a curved interface (drop/air) before reaching the detector. Accordingly, the Raman signal is improved with the hanging drop configuration.

2.3 Characterisation procedure

The pH evolution of the drops was measured using a hot line CupFET probe (Sentron) introduced in the crystallisation chamber through a lateral hole. Confocal Raman microspectroscopy was used to monitor the evolution of CaP precipitation both inside the drop and also at the interface between the drop and the cover glass (Figure 1). Firstly, the spectrum of the precipitates obtained just after mixing $Ca(CH_3COO)_2$ and $(NH_4)_2HPO_4$ solutions (hereafter, this instant is referred to as t_0) was collected. Subsequently, and once the "crystallisation mushroom" was sealed, optical micrographs and the corresponding Raman spectra were sequentially acquired every 15 minutes during the first 12 hours of experiment. Afterward, the spectra were collected every 12 hours until the completion of the experiment (7 days). Raman spectra were collected with a LabRAM-HR spectrometer with backscattering geometry (Jobin-Yvon, Horiba, Japan). The excitation line was provided by a diode laser emitting at a wavelength of 532 nm and a Peltier cooled charge-couple device (CCD) (1064x256 pixels) was used as detector. Spectrometer resolution is better than 3 cm^{-1}. For each acquisition and depending on the quality of the spectra, signal average of two or three spectra and acquisition time between 100 and 500 s was performed. The spectra were linearly base-line corrected for clarity.

Furthermore, the precipitates derived after seven days were repeatedly washed with ultrapure water by centrifugation, freeze-dried for 12h at -52 °C and stored at room temperature. They were characterised by X-Ray powder diffraction (XRPD), Raman spectroscopy and Transmission electron microscopy (TEM). The XRPD diffractograms were collected using a Cu Kα radiation (k = 1.5418 Å) on a PANalytical X'Pert PRO diffractometer equipped with a PIXcel detector operating at 45 kV and 40 mA. For the diffracted beam an automatic-variable anti-scatter slit with an irradiated length of 10 mm was used. The 2θ range was from 5° to 80° with a step size of (2θ) 0.039°. TEM images as well as selected area electron diffraction (SAED) were performed with a STEM Philips CM 20 microscope operating at 80 kV. The powdered samples were ultrasonically dispersed in ultrapure ethanol and then a few drops of the slurry were deposited on conventional copper microgrids.

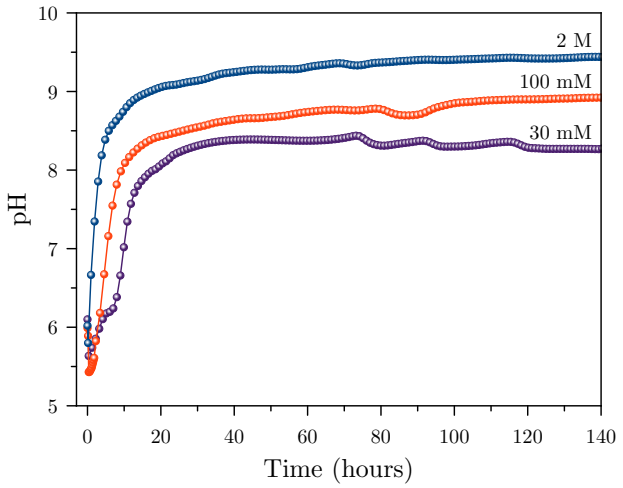

Fig. 2 pH evolution in the drops by diffusion of NH_3 and CO_2 gases released from solutions of NH_4HCO_3 with three different concentrations.

3 Results

3.1 pH Evolution

As previously described, the pH plays a key role in the stability, and therefore in the crystallisation process of the CaP.[12,13] Figure 2 shows the pH evolution in the drops during seven days of vapour diffusion working at 30 mM, 100 mM and 2 M NH_4HCO_3 concentrations. The initial pH in the drop just after mixing the $Ca(CH_3COO)_2$ and $(NH_4)_2HPO_4$ solutions was 6.10. Once the "crystallisation mushroom" was sealed the pH decreased to around 5.5. After 20 minutes of vapour diffusion, the pH started to increase until reaching an asymptotic value. This trend was similar for all the tested NH_4HCO_3 concentrations but the slope of the pH increase curve became more pronounced at higher NH_4HCO_3 concentrations. In addition, both the final pH value and the time needed to reach it, strongly depend on the concentration of NH_4HCO_3. Indeed, the final pH values 8.38, 8.90 and 9.42 were measured after 44, 110 and 130 hours when using 30 mM, 100 mM and 2 M NH_4HCO_3 solutions, respectively.

3.2 Phase evolution in the bulk of the drop

Time-dependent Raman spectra collected focusing just in a focal plane at the centre of the drops for the three NH_4HCO_3 concentrations are depicted in Figure 3. In addition, the assignments of the Raman peaks to the vibrational modes of the CaP and $CaCO_3$ phases are summarized in table 1. The spectrum recorded at t_0 mainly shows two peaks appearing at *ca.* 927 and 952 cm^{-1}. The former is due to the C-C stretching mode of acetate ions in solution whereas the lat-

Table 1 Raman shift (cm^{-1}) of the main peaks used to identify the CaP and $CaCO_3$ phases.

Assignments	ACP[a]	DCPD[b]	OCP[b]	HA[b]	Calcite[c]
$\nu_s PO_4$	952	985, 878	958, 965	961	-
$\nu_s HPO_4$	-	-	1010	-	-
$\delta_s CO_3$	-	-	-	-	711
$\nu_s CO_3$	-	-	-	-	1085

[a] Reference [39]
[b] Reference [23]
[c] Reference [40]

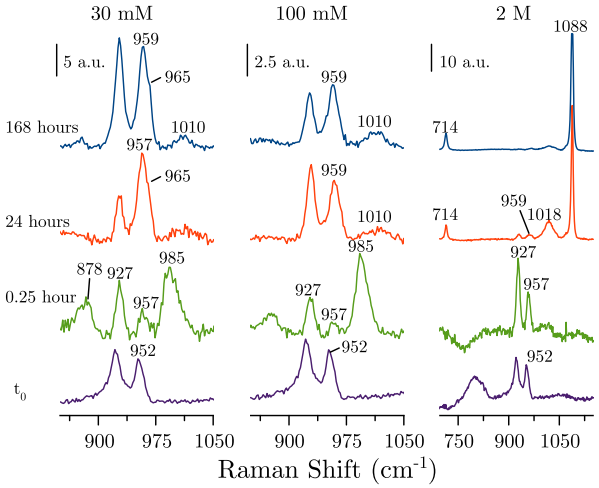

Fig. 3 Time-dependent *in situ* Raman spectra collected for the drops inside the "crystallisation mushroom" using 30 mM, 100 mM and 2 M NH_4HCO_3 concentrations.

ter is assignable to the symmetric stretching mode of phosphate groups.[41] The Raman shift of this band indicates the formation of an amorphous calcium phosphate (ACP).[39] This finding confirms the TEM observations of the first precipitates obtained when the SDVD method was used.[31] Afterwards, coinciding with the decrease of pH, big platelets started to grow in the drops. Indeed, the Raman spectra collected at 0.25 hour reveal peaks at *ca.* 878, 985 and 957 cm^{-1} (Figure 3), irrespective of the NH_4HCO_3 concentration. They are ascribed to the symmetric stretching modes ($\nu_s PO_4$) of phosphate groups in DCPD and OCP, respectively (table 1).[23] It indicates the presence of both phases in the bulk of the drop. Subsequently, DCPD crystals began to dissolve disappearing after 6, 5 and 1 hours for the experiments carried out under 30 mM, 100 mM and 2 M (table 2). In fact, after 24 hours, the Raman spectra for the experiment with 30 mM solution show a main peak at *ca.* 958 cm^{-1} with a shoulder at 965 cm^{-1} as well as a broad band at 1010 cm^{-1}. They can be ascribed, respectively, to the P-O symmetric stretching modes of PO_4 ($\nu_s PO_4$) and HPO_4 ($\nu_s HPO_4$) groups in OCP crystals (table 1).[23] Basically the

Table 2 CaP detected in the bulk of the drops by *in situ* Raman microspectroscopy.

$[NH_4HCO_3]$ (M)	time (hours)	Phase detected
	t_0	ACP
	0.25	DCPD and OCP
0.03	6	OCP
	24	OCP and cAp
	168	OCP and cAp
	t_0	ACP
	0.25	DCPD and OCP
0.1	5	OCP
	24	cAp and OCP
	168	cAp and OCP
	t_0	ACP
	0.25	DCPD and OCP
2	1	OCP
	24	cAp, OCP and calcite
	168	calcite

same spectrum is attained after 168 hours. Regarding to the experiment performed with 100 mM, similar behaviour is observed but the shoulder at 965 cm^{-1} does not appear. This point in conjunction with the fact that the apatite phase exhibits its main peak usually at *ca.* 961 cm^{-1} [23] may suggest the presence of both phases. However, they cannot be quantified because of the overlapping of their main peaks (table 1). On the other hand, the increase in concentration of the NH_4HCO_3 solution up to 2 M leads to a completely different evolution, as it is shown in Figure 3. The spectrum collected at 24 hours exhibits Raman peaks at *ca.* 714 and 1088 cm^{-1} that belongs, respectively, to the symmetric deformation ($\delta_s CO_3$) and symmetric stretching ($\nu_s CO_3$) modes of carbonate groups in calcite.[40] Additionally, the peak at *ca.* 958 cm^{-1} can be due to OCP and/or HA phases whereas the broad band at 1018 cm^{-1} is ascribed to the C-OH stretching mode ($\nu C-OH$) of bicarbonate ions in solution[42] coming from the diffusion of CO_2. After 168 hours, only the Raman peaks of calcite are drawn. Calcite crystals (see graphical abstract) exhibited a well-faceted morphology resembling those of calcite produced in the presence of certain carboxylic acids[43] or acetic acid.[44] The crystals appeared elongated along the *c*-axis, and bound by rhombohedral {104} and prismatic {110} and {100} faces, although some of them are intergrown crystals. Table 2 summarizes the main phases detected by Raman microspectroscopy as a function of the precipitation time for each concentration of NH_4HCO_3 used.

3.3 Phase evolution at the drop/glass interface

The phase evolution for the experiment performed with 100 mM NH_4HCO_3 was also studied by confocal Raman microspectroscopy but focusing on the drop/glass interface . The

This journal is © The Royal Society of Chemistry [year]

optical micrographs in Figure 4 illustrate, as part of the process, the growth of big DCPD platelets (A-B) and their further dissolution (C) until they completely disappear after 6 hours (Figure 4). Furthermore, a serie of time-dependent spectra of the process is shown in (Figure 4). The spectra collected at 0.25 and 1 hour reveal the presence of DCPD[23] as unique phase. There are no peaks corresponding to ACP. After 5 hours, a peak at 958 cm^{-1} emerges indicating the appearance of OCP in the solution. After 6 hours, only the peak at *ca.* 959 cm^{-1} is noticed, likely indicating the presence of both OCP and apatite phases, indistinguishable by Raman spectroscopy. Therefore, the phase transformations in the bulk are slightly faster than at the interface. The inset in figure 4 represents the plot, as a function of time, of the integrated intensities of the bands at 985 cm^{-1} (DCPD) and 958 cm^{-1} (OCP) as well as the pH evolution. In the early stages, the ACP rapidly dissolved and the DCPD phase nucleated and grew during approximately 1 hour. During this process the pH decreased from 6.10 to 5.40. Afterwards, DCPD began to dissolve. Only when it was almost dissolved after 5 hours (at pH around 6.5), the OCP nucleated and started to grow.

3.4 Characterisation of the freeze-dried samples

The freeze-dried precipitates (obtained after 168 hours of vapour diffusion) were also characterised by TEM, XRPD, Raman and Infrared Spectroscopies. Figure 5 A and B show TEM micrographs of the sample precipitated under 30 and 100 mM solutions, respectively. At the lower concentration, plate-like crystals composed of OCP, as pointed out by the SAED pattern[31], with size ranging between 200 and 600 nanometres can be observed. Furthermore, needle-like nanoapatite with length between 20 and 100 nanometres are also distinguished. Figure 5B reveals mainly nanosized apatite and only few and smaller OCP crystals. These results confirm that both phases coexist after 7 days for both conditions, but with a lower OCP amount in the second case. Figure 5 C and D represent the XRPD diffractograms and Raman spectra of the sample precipitated under different NH_4HCO_3 concentrations. The diffractograms of the precipitate powders formed in the presence of 30 and 100 mM exhibit broad reflections ascribed to HA (ASTM Card file No 9-432). The broadening of the diffraction peaks indicates a relatively low crystallinity degree, similar to biological apatites. In addition, the 020 and $\bar{1}01$ reflections (marked with an asterisk) appearing at lower 2θ angles are due to OCP (ASTM card file No. 26-1056). The fact that the latter reflections are much weaker for the sample precipitated under 100 mM NH_4HCO_3 solutions confirms that the amount of OCP is lower for this sample, as also TEM observations pointed out. Infrared spectra of these sample (not shown) display typical bands of A- and B-type carbonate substitutions into the apatitic crystal lattice, as previously reported

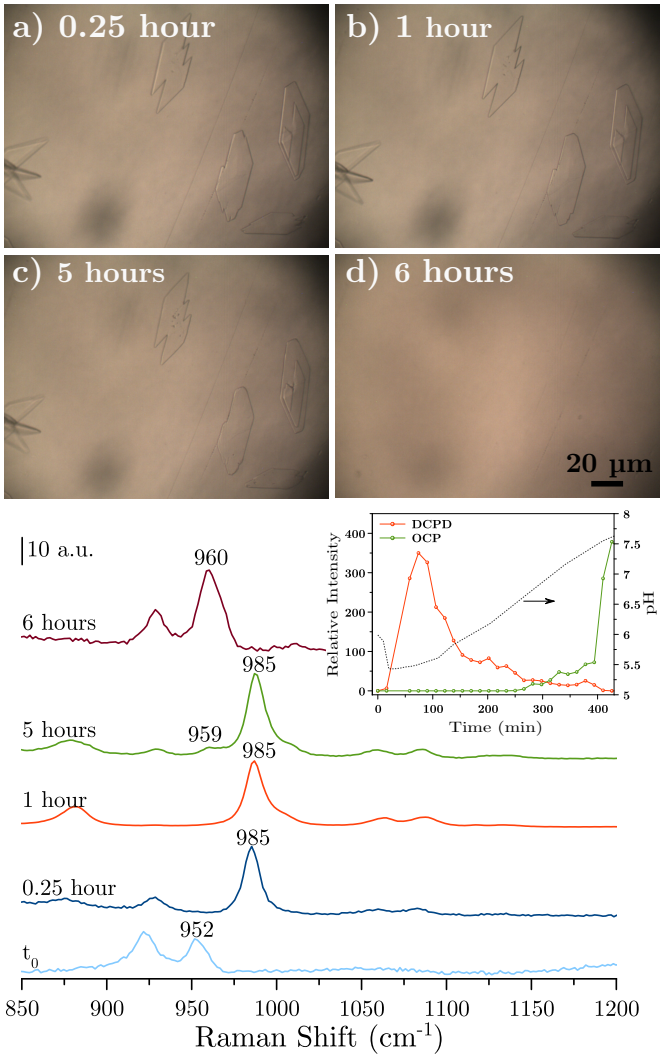

Fig. 4 Optical micrographs showing DCPD evolution at the drop/glass interface working with 100 mM NH_4HCO_3 solution. Selected time-dependent *in situ* Raman Spectra. The inset shows the plot as a funtion of time of the integrated intensities of DCDP (985 cm^{-1}) and OCP (958 cm^{-1}) Raman peaks calculated from the time-dependent serie. For the sake of comparison between spectra collected at different instants, the intensities have been divided by the integrated intensity of the *νCC* mode of acetate ions in solution appearing at *ca.* 927 cm^{-1}. Note: the spectrum at t_0 was collected in the same conditions than in figure 3.

for cAp derived under similar conditions by SDVD method.[32] On the other hand, XRPD pattern (c in Figure 5C) and Raman spectrum (c in Figure 5B) collected for the sample grown in the presence of the 2 M solution indicate that calcite is the unique phase (ASTM card file No. 5-586).

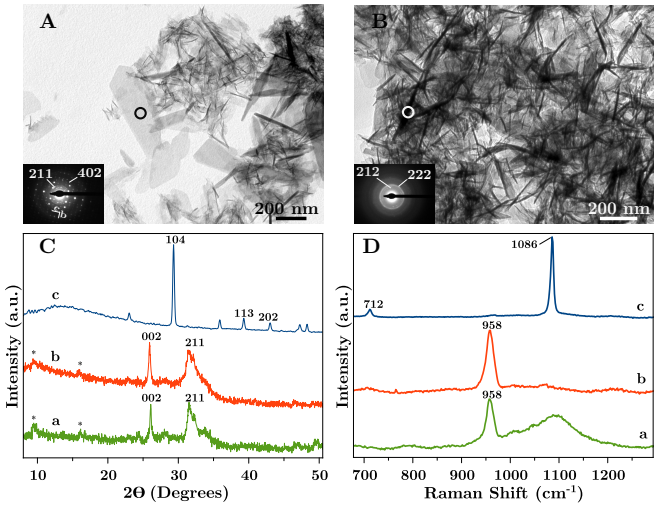

Fig. 5 TEM micrographs of CaP crystallised under 30 mM (A) and 100 mM (B). The insets show SAED patterns collected for the crystals marked in each figure. XRPD diffractograms (C) and Raman spectra (D) acquired for the dried powders grown in the presence of (a) 30 mM, (b) 100 mM and (c) 2 M of NH_4HCO_3 solutions.

4 Discussion

The results of *in situ* time-dependent Raman microspectroscopy and pH evolution complemented with TEM, XRPD and Raman spectroscopy of the final precipitates evidenced a same CaP precipitation pathway during the first 24 hours of vapour diffusion to obtain nanocrystalline apatite. Nonetheless, they indicated different kinetics of phase transformation depending on the NH_4HCO_3 concentration. This pathway consists in the initial precipitation of ACP nanoparticles whose lifetime were a few minutes, then the nucleation, growth and further dissolution of big DCPD platelets (7, 6 and 3 hours of experiment, when using 30 mM, 100 mM and 2 M NH_4HCO_3 solutions), followed by nucleation and growth of OCP crystals, that coexist with nanocrystalline apatites. The precipitation mechanism was more clearly revealed in the experiment at 100 mM, by focusing at the drop/glass interface (Figure 4). A dissolution-reprecipitation mechanism for the ACP-DCPD and DCPD-OCP transformations explain the findings. The coexistence of the OCP and apatite phases, which are indistinguishable by Raman spectroscopy, was clearly revealed by TEM observations. Conversely, using the most concentrated NH_4HCO_3 solution, OCP not only coexists with the apatite but also with calcite. In this experiment we also noted that kinetic of phase transformation in the bulk of the drop was slightly faster than at the drop/glass interface. It was most likely due to the heterogeneity of the diffusion/dissolution rate of CO_2 and NH_3 through the drop, that created a gradient of supersaturation decreasing from the air/drop interface to the drop/glass interface.

Some authors suggested that transformation of OCP into HA takes place by a hydrolysis process.[45] However, this process cannot explain why the apatite phase is obtained with nanosized dimensions. In a previous paper, based on experimental observations we suggested that OCP most likely acts as temporal template for the formation of carbonate apatite nanocrystals[31] in the same way as $Na_3(cit)\cdot 2H_2O$ acted during the precipitation of this material from a Ca/citrate/phosphate solution at pH=8.3.[21] The initial precipitation of this calcium citrate salt acted as temporal template for the formation of the apatite phase with nanometric size.[21] In the absence of this template, crystals grew up to submicrometric or micrometric sizes. The role of the template basically consists on the stabilization of the heterogeneously nucleated apatite within the nanometric size range. In fact, the precipitation of apatite phase, usually takes place at very high values of the thermodynamic supersaturation, which leads to the formation of critical nuclei of extremely small sizes. The decrease of free energy in that system can be produced not only by growth but also by primary aggregation of the nascent particles with nanometre size. The presence of a template might interact with the primary particles formed by heterogeneous nucleation, stabilizing them and, thus, minimizing their aggregation tendency. Hence, nanosized crystals are formed. From the biological point of view, both DCPD and OCP have repeatedly found as precursor of nanocrystalline apatites in *in vitro* crystallization but *in vivo* studies rarely show the presence of these phases.[18]. Nevertheless, evidences of the OCP role as template were only detected in experiments of vapour diffusion.[31–33]

Another interesting observation is the formation of calcite in the experiment carried out at 2M NH_4HCO_3. Comparing the pH-evolution curves in the three experiments, they display a more pronounced slope as well as a higher final pH as the NH_4HCO_3 concentration increased. The different slopes reflect different diffusion rates of gases through the drops, that can be the key factor to explain the formation of calcium carbonate instead of calcium phosphate. In the experiment using the highest concentration of NH_4HCO_3, the partial pressures of released NH_3 and CO_2 gases were much higher and therefore the diffusion rates into the aqueous drops. Under these circumstances the kinetics of CaP transformation increases, reducing the lifetime of each one of the phases. After attaining the saturation of gas in drops, the ionic activity product of calcium carbonate $[(aCa^{2+})\cdot(aCO_3^{2-})]$ also increased rapidly and overpassed the solubility product of calcite, the less soluble phase of calcium carbonate (log K_{sp}(calcite) = -8.453). This process was produced at a rate higher than the one at which the ionic activity product of CaP would exceed the solubility product of the OCP and apatite phases. It leads to the precipitation of calcite instead of a calcium phosphate phase

This journal is © The Royal Society of Chemistry [year]

in this step of the process, thus, highlighting the role of the kinetic control.

5 Conclusions

Confocal Raman microspectroscopy allowed to monitor *in situ* the evolution of CaP precipitation in HDVD experiments, both at the drop/glass interface and in the bulk of the drop. The results described above pointed out that the pH increase rate plays a key role on the CaP crystallisation and phase transformation. This rate only depends on the concentration of NH_4HCO_3 used. ACP was found just after mixing the calcium and phosphate solutions. Then, it transforms to DCPD, which subsequently dissolves and recrystallises into OCP. This phase transformation depends on the concentration of NH_4HCO_3: the higher the concentration the faster the transformation. For the experiments carried out with 30 mM and 100 mM NH_4HCO_3 solutions, the system evolves to needle-like nanosized cAp that closely mimic biological nanocrystalline apatites with low degree of maturation. These nanocrystals appeared coexisting with plate-shaped OCP crystals which probably play the role of temporal template for the in vitro nanoapatite crystallisation. On the other hand, for the highest concentration (2M), in the first day, OCP, cAp and calcite coexisted in the drop. Nonetheless, after 24 hours, large calcite crystals elongated along the *c*-axis were only identified. For the experiments at 100 mM NH_4HCO_3, the whole CaP precipitation process at the drop/glass interface was slightly slower than in the bulk of the drop.

Acknowledgements

This work was carried out within the framework of the projects MAT2011-28543, "Factoría de Cristalización (Consolider Ingenio 2010) (Spanish Ministerio de Ciencia e Innovación (MICINN)) and Excellence project RNM5384 of Junta de Andalucía.

References

1 S. Dorozhkin, *Materials*, 2009, **2**, 399–498.
2 M. J. Arellano-Jiménez, R. García-Garcia and J. Reyes-Gasga, *J. Phys. Chem. Solids*, 2009, **70**, 390–395.
3 M. Ashok, S. N. Kalkura, N. M. Sundaram and D. Arivuoli, *J. Mater. Sci.-Mater. M.*, 2007, **18**, 895–898.
4 K. Ganesan, A. Kovtun, S. Neumann, R. Heumann and M. Epple, *J. Mater. Chem.*, 2008, **18**, 3655–3661.
5 S. Koutsopoulos and E. Dalas, *Langmuir*, 2001, **17**, 1074–1079.
6 S. Lazic, *J. Cryst. Growth*, 1995, **147**, 147–154.
7 X. Lu, Y. B. Wang, J. X. Wang, S. X. Qu, J. Weng, R. L. Xin and Y. Leng, *J. Cryst. Growth*, 2006, **297**, 396–402.
8 R. Mazzé, *Periodico di Mineralogia*, 2009, **78**, 19–43.
9 D. Rabadjieva, R. Gergulova, R. Titorenkova, S. Tepavitcharova, E. Dyulgerova, C. Balarew and O. Petrov, *J. Mater. Sci.-Mater. M.*, 2010, **21**, 2501–2509.
10 L. M. Rodriguez-Lorenzo and M. Vallet-Regi, *Chem. Mater.*, 2000, **12**, 2460–2465.
11 R. Xin, Y. Leng and N. Wang, *J. Cryst. Growth*, 2006, **289**, 339–344.
12 M. J. J. M. van Kemenade and P. L. de Bruyn, *J. Colloid Interf. Sci.*, 1987, **118**, 564–585.
13 L. Wang and G. H. Nancollas, *Chem. Rev.*, 2008, **108**, 4628–4669.
14 D. Eichert, *Nanocrystalline Apatite-Based Biomaterials*, Nova Science Pub Incorporated, 2009.
15 S. Mann, *Biomineralization: principles and concepts in bioinorganic materials chemistry*, University Press, Oxford, 2001.
16 R. Z. LeGeros, *Prog. Cryst. Growth Ch.*, 1981, **4**, 1–45.
17 H. A. Lowenstam and S. Weiner, *On Biomineralization*, University Press, Oxford, 1989.
18 M. S.-A. Johnsson and G. H. Nancollas, *Crit. Rev. Oral Biol. Med.*, 1992, **3**, 61–82.
19 N. Nassif, F. Gobeaux, J. Seto, E. Belamie, P. Davidson, P. Panine, G. Mosser, P. Fratzl and M.-M. Giraud Guille, *Chem. Mater.*, 2010, **22**, 3307–3309.
20 N. Nassif, F. Martineau, O. Syzgantseva, F. Gobeaux, M. Willinger, T. Coradin, S. Cassaignon, T. Azas and M. M. Giraud-Guille, *Chem. Mater.*, 2010, **22**, 3653–3663.
21 A. López-Macipe, J. Gómez-Morales and R. Rodríguez-Clemente, *Adv. Mater.*, 1998, **10**, 49.
22 J. M. Delgado-López, M. Iafisco, I. Rodríguez, A. Tampieri, M. Prat and J. Gómez-Morales, *Acta Biomaterialia*, 2012, **8**, 3491 – 3499.
23 S. Koutsopoulos, *J. Biomed. Mater. Res.*, 2002, **62**, 600–612.
24 B. Palazzo, M. Iafisco, M. Laforgia, N. Margiotta, G. Natile, C. Bianchi, D. Walsh, S. Mann and N. Roveri, *Adv. Funct. Mater.*, 2007, **17**, 2180–2188.
25 S. Manara, F. Paolucci, B. Palazzo, M. Marcaccio, E. Foresti, G. Tosi, S. Sabbatini, P. Sabatino, G. Altankov and N. Roveri, *Inorg. Chim. Acta*, 2008, **361**, 1634–1645.
26 M. Iafisco, M. Marchetti, J. Gómez-Morales, M. A. Hernández-Hernandez, J. M. García-Ruiz and N. Roveri, *Cryst. Growth Des.*, 2009, **9**, 4912–4921.
27 D. G. Wang, C. Z. Chen, H. Ting and T. Q. Lei, *J. Mater. Sci.-Mater. M.*, 2008, **19**, 2281–2286.
28 Y. Z. Wang and Y. Fu, *Mater. Lett.*, 2011, **65**, 3388–3390.
29 W. Y. Zhou, M. Wang, W. L. Cheung, B. C. Guo and D. M. Jia, *J. Mater. Sci. Mater. Med.*, 2008, **19**, 103–110.
30 S. V. Dorozhkin, *Acta Biomater.*, 2010, **6**, 715–734.
31 J. Gómez-Morales, J. M. Delgado-López, M. Iafisco, A. Hernández-Hernandez and M. Prat, *Cryst. Growth Des.*, 2011, **11**, 4802–4809.
32 M. Iafisco, J. Gómez-Morales, M. A. Hernández-Hernandez, J. M. García-Ruiz and N. Roveri, *Adv. Eng. Mater.*, 2010, **12**, B218–B223.
33 M. Iafisco, J. M. Delgado-López, J. Gómez-Morales, M. A. Hernández-Hernandez, I. Rodríguez-Ruiz and N. Roveri, *Cryst. Res. Technol.*, 2011, **46**, 841–846.
34 J. Gómez-Morales, A. Hernández-Hernandez, G. Sazaki and J. M. García-Ruiz, *Cryst. Growth Des.*, 2010, **10**, 963–969.
35 A. Hernández-Hernandez, A. B. Rodríguez-Navarro, J. Gómez-Morales, C. Jimenez-Lopez, Y. Nys and J. M. García-Ruiz, *Cryst. Growth Des.*, 2008, **8**, 1495–1502.
36 A. Hernández-Hernandez, J. Gómez-Morales, A. B. Rodríguez-Navarro, J. Gautron, Y. Nys and J. M. García-Ruiz, *Cryst. Growth Des.*, 2008, **8**, 4330–4339.
37 C. Krafft and V. Sergo, *Spectroscopy*, 2006, **20**, 195–218.
38 C. Krafft, *Anal. Bioanal. Chem.*, 2004, **378**, 60–62.
39 G. R. Sauer, W. B. Zunic, J. R. Durig and R. E. Wuthier, *Calcif. Tissue*

Int., 1994, **54**, 414–420.
40 S. Gunasekaran, G. Anbalagan and S. Pandi, *J. Raman Spectrosc.*, 2006, **37**, 892–899.
41 G. Socrates, *Infrared and Raman Characteristic Group Frequencies*, John Wiley & Sons, Chichester, 2001.
42 N. Wen and M. H. Brooker, *J. Phys. Chem.*, 1995, **99**, 359–368.
43 N. Wada, K. Kanamura and T. Umegaki, *J Colloid Interf. Sci.*, 2001, **233**, 65 – 72.
44 L. Pastero, E. Costa, M. Bruno, M. Rubbo, G. Sgualdino and D. Aquilano, *Cryst. Growth Des.*, 2004, **4**, 485–490.
45 A. Bigi, E. Boanini, G. Cojazzi, G. Falini and S. Panzavolta, *Cryst. Growth Des.*, 2001, **1**, 239–244.

This journal is © The Royal Society of Chemistry [year]